Experimental test of virtual photon theory

W. R. Dodge, E. Hayward, and E. Wolynec*
National Bureau of Standards, Washington, D.C. 20234
(Received 25 August 1982)

An isochromat of the $E1$ virtual photon spectrum has been measured by counting the number of ground-state protons emitted by the 16.28 MeV isobaric analog state in ^{90}Zr as a function of incident electron energy in the range 17—105 MeV. The experimental results reproduce well the distorted wave Born approximation spectra for a point Zr nucleus for electron energies up to 30 MeV. A radiator was used for electron energies of 60—100 MeV to measure the photodisintegration plus electrodisintegration cross section. These results showed that the Davies-Bethe-Maximon bremsstrahlung cross section magnitude yields the same result as the electrodisintegration results below 30 MeV where size corrections for the finite extent of the nucleus are minimal. As E_0 increases to 105 MeV the need for such corrections becomes manifest. Several such corrections are discussed. As by-products of this study the quantity $\Gamma_\gamma\Gamma_{p_0}/\Gamma$ was determined to be 63.8±1.9 eV or 66.1±2.0 eV depending on the virtual photon spectrum used in analysis. The $\Gamma_{p_2}/\Gamma_{p_0}$ ratio was also determined to be 0.58±0.02. Combining these results yields for Γ_γ 100.8±5.0 eV or 104.4±5.2 eV.

NUCLEAR REACTIONS ^{90}Zr(e,p_0), $E=16.28$ MeV, measured $\sigma(e,p_0)$ vs E_0, deduced $\Gamma_{p_0}\Gamma_\gamma/\Gamma$, compared with virtual photon theory. Measured $\Gamma_{p_2}/\Gamma_{p_0}$, deduced Γ_γ.

I. INTRODUCTION

During the last decade the study of the giant multipole resonances together with the emergence of the distorted wave Born approximation (DWBA) virtual photon calculations of Onley, Wright, and collaborators[1,2] have jointly stimulated a renaissance of interest in electrodisintegration experiments. Early calculations of the $M1$, $E2$, and $E3$ virtual photon spectra in plane wave Born approximations showed that these higher multipole spectra were greatly enhanced relative to the $E1$ spectrum. The enhancement was understood as resulting from the momentum dependence of the higher multipole cross sections and the fact that in the electron scattering event the momentum transfer to the nucleus can greatly exceed the energy transfer. None of these early calculations included a full treatment of Coulomb distortions because the existing computers were so limited. Consequently, the early virtual photon spectra were grossly underestimated for all but the lightest nuclei.

Gargaro and Onley[1] were the first to calculate the virtual photon spectra taking into account the distortion of the incoming and outgoing electron waves in the Coulomb field of a point nucleus. These calculations showed that the enhancement of the higher multipole virtual photon spectra, already seen in PWBA calculations, was greatly increased as the atomic number of the nucleus increased.

The enhancement of the $E2$ relative to the $E1$ DWBA virtual photon spectra has recently been exploited in several electrodisintegration experiments.[3–7] In these experiments the connection betweeen the electrodisintegration cross section $\sigma_{e,x}(E_0)$ and the photonuclear cross section $\sigma_{\gamma,x}(E)$ was utilized:

$$\sigma_{e,x}(E_0)=\int\sum_{\lambda l}\sigma_{\gamma,x}^{\lambda l}(E)N^{\lambda l}(E_0,E,Z)\frac{dE}{E}\ . \tag{1}$$

Here $N^{\lambda l}(E_0,E,Z)/E$ stands for the number of virtual photons of multipolarity l exchanged with a nucleus of atomic number Z when an electron of energy E_0 produces an excitation of energy E. Equation (1) is based on the assumption that the reduced transition probabilities for photodisintegration and electrodisintegration, $B(El,E)$, and $B(El,q)$, are equal. Here q is the momentum transferred to the nucleus in electrodisintegration. This assumption is exact as $q\rightarrow E$ but surely fails for $q\gg E$.

Few experimental checks[8] of the virtual photon spectra have been made and these have certainly not been extensive, nor the conclusions definite.[9] All have integrated over the $E1$ giant resonance and hence included a broad range of virtual photon energies and perhaps multipolarities. Only $E1$ excitations have been explored and none extended beyond 30 MeV so that there has been no real opportunity to demonstrate the failure of the long wavelength approximation on which Eq. (1) is based.

We have measured the cross section for excitation of the 16.28 MeV, 1^- analog state in ^{90}Zr with real and virtual photons in the energy range 17 to 105 MeV. This measurement serves as a check on the shape of the $E1$ virtual photon spectrum at the 2—3% level. The failure of the long wavelength approximation has been observed for electron energies above ~30 MeV and several "nuclear size effect" corrections postulated. In addition, we have used a radiator for electron energies above 60 MeV as a check on our experiment for an interaction in which there are no nuclear size effects and to compare the magnitude of the bremsstrahlung cross section with the virtual pho-

ton spectrum.

We have used the 1^- isobaric analog state in ^{90}Zr for this work. It has already been thoroughly studied using the (e,p) (Ref. 10) and ^{89}Y (p,γ_0) (Refs. 11 and 12) reactions. This level has a proton width of about 75 keV, a ground-state radiation width of about 100 eV, and decays by proton emission to the ground and 1.51 MeV second-excited state of ^{89}Y. The ground-state and excited state[10] protons have a typical dipole angular distribution,[12]

$$a_0P_0(\cos\theta_p)+a_2P_2(\cos\theta_p)\ .$$

II. THE EXPERIMENT

The apparatus used was the same as in earlier reported experiments[3,4] with the following exceptions: (1) the data logging computer and all related interface and input modules were replaced with a new minicomputer and CAMAC modules, and (2) three of five previously used 2.3-cm circular semiconductor focal plane counters were replaced with 1.5×4-cm rectangular counters. The use of rectangular counters in the focal plane insures that all areas of the target illuminated by the beam are viewed with equal efficiency.

Figure 1 shows a plot of the spectrum of protons emitted at 90° by a 2 mg/cm^2 target of ^{90} Zr bombarded by 60 MeV electrons. It is very similar to spectra already published by Shoda *et al.*[10] which helped us to identify peak *A* as the 7.9 MeV group populating the ground state of ^{89}Y from the 16.28 MeV state in ^{90}Zr. Peak *B* results from the protons from this same state populating the second excited state of ^{89}Y at 1.51 MeV.

The prominent peak *A* was then studied in detail as a function of incident electron energy. Seven magnetic fields were chosen so as to delineate points 50 keV apart on this peak in the proton spectra. Figure 2 shows the spectrum obtained using 24 MeV incident electrons. The observed width has roughly equal contributions from the natural proton width, the spectrometer focal plane momentum bite, and the energy straggling in the target. A Gaussian plus quadratic function was least-squares fitted to the data. The slight asymmetry exhibited by the peak has been attributed by Hasinoff *et al.*[12] to interference between this state and the giant dipole resonance. The lower part of the figure shows the peak after subtracting the continuum, the area of which was obtained by a numerical integration of the actual experimental data. These integrations yielded the differential cross section $d\sigma_{e,p_0}/d\Omega$ that results in the emission of 7.9 MeV protons at 90°. These differential cross sections were measured for electron energies in the range 17—105 MeV and are plotted as a function of incident electron energy E_0 in Fig. 3. The statistical errors are smaller than the size of the points.

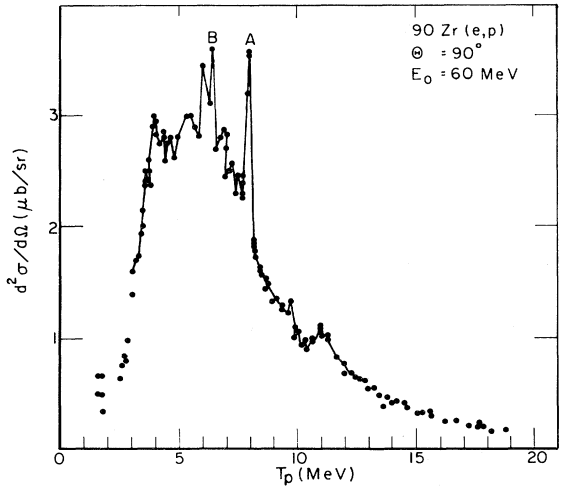

FIG. 1. The spectrum of protons emitted when a 2.03 mg/cm^2 ^{90}Zr target is bombarded by 60 MeV electrons.

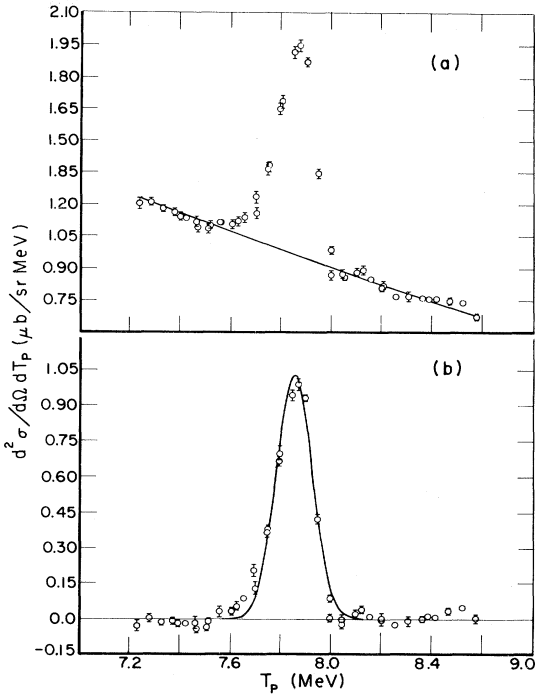

FIG. 2. The data used to determine the differential cross section $d\sigma_{e,p_0}/d\Omega$ for 24 MeV incident electrons. A Gaussian plus quadratic function was fitted to the data. The curve in (a) is the quadratic function which fits the continuum. The curve in (b) is the Gaussian function after subtraction of the quadratic function. These data have not been corrected for energy loss ($\sim$40 keV) in the target.

At electron energies of 60, 70, 80, 90, and 100 MeV the same proton spectra were measured using a tantalum radiator, 0.1356 mg/cm^2 in thickness, located 7.6 cm ahead of the target. In addition, at 60 and 100 MeV, a 0.2172 g/cm^2 tantalum radiator was used as a check on the effects of electron energy loss and multiple scattering in the radiator. The measured cross section consists of the electrodisintegration cross section plus the contribution produced by the real photons generated in the radiator. The difference between the areas measured with and without the radiator divided by the number of 16.28 MeV bremsstrahlung photons generated in the radiator is the differential photoproton cross section $d\sigma_{\gamma p_0}/d\Omega$. A slight adjust-

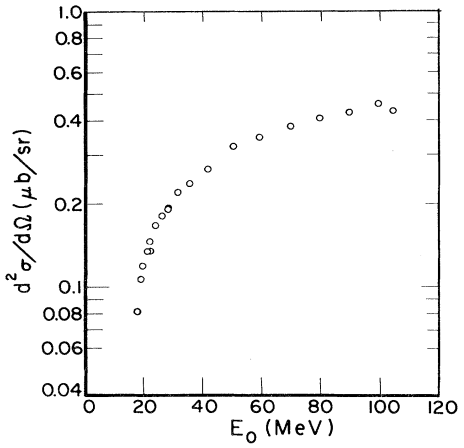

FIG. 3. $d\sigma_{e,p}/d\Omega$ as a function of electron energy E_0.

ment has been made for the energy loss of the electrons in the radiator.

The largest experimental uncertainty is associated with the target thickness. We have used the thickness obtained by weighing, 2.03 mg/cm^2, to calculate the cross sections. During the course of the experiment we observed slow variations in the counts per beam charge which we were able to identify as arising from changes in the effective target thickness produced by beam heating induced "puckering" of the target foil. We found that consistent and reproducible results could be obtained by averaging values of the cross section measured with the plane of the target at $\pm 45°$ with respect to the spectrometer ($+45°$ and $+135°$ with respect to the electron beam). This procedure averaged to zero the small changes in the target thickness due to electron beam heating. The two values obtained at $\pm 45°$ were often the same but sometimes differed by as much as three or four percent. The points plotted in Fig. 3 at 17.2, 18.2, 19.2, and 21.2 MeV were measured using a different target a year before this procedure was established and have been adjusted upward by a factor of 1.017 to match those at 21.2 and 22.2 MeV.

Measurements made at electron energies near the threshold for the excitation of this state indicated that the energy calibration of our electron beam line was in error by roughly 0.8 MeV at 17.5 MeV. Because of this discrepancy, we repeated the energy calibration of our beam line. The field in the magnet that defines the electron energy was compared with the field in the spectrometer by elastic electron scattering at 16, 18, 20, 22, 24, 26, 30, 40, 60, 80, and 100 MeV, the ultimate calibration of the spectrometer being referred to a National Bureau of Standards standard ^{241}Am α-particle source. The present energy scale is known to about ± 60 keV.

During the course of the measurements it became apparent that with very little extra effort the relative intensities of the peaks A and B of Fig. 1 could be measured. Accordingly, very detailed spectra in the proton kinetic energy range 5–8.8 MeV were measured for incident electron energies of 22 and 28 MeV. The spectrum obtained using 22 MeV electrons is shown in Fig. 4. The average value for $\Gamma_{p_2}/\Gamma_{p_0}$ obtained from these two experiments is 0.58 ± 0.02 where the error is based only on counting statistics. This result is to be compared with 0.70 obtained by Shoda.[10]

III. RESULTS

Since we are studying the electric dipole excitation of a discrete level, Eq. (1) simplifies to

$$\sigma_{e,p_0}(E_0)=\frac{N^{E1}(E_0,E,Z)}{E}\int \sigma_{\gamma,p_0}(E)dE \ , \tag{2}$$

where the integral is now over the photonuclear absorption cross section into the level at 16.28 MeV that results in protons populating the ground state of ^{89}Y, or

$$\int \sigma_{\gamma,p_0}(E)dE=(\pi\lambda\!\!\!^{-})^2\frac{2I+1}{2I_0+1}\frac{\Gamma_{p_0}\Gamma_\gamma}{\Gamma} \ , \tag{3}$$

where I and I_0 are the spins of the excited and ground states.

Dodge and Barber[13] have already shown in the PWBA that if the photonuclear cross section differential in angle is

$$d\sigma_{\gamma,p}/d\Omega=a_0P_0(\cos\theta_p)+a_2P_2(\cos\theta_p) \ , \tag{4}$$

then the corresponding electrodisintegration cross section is

$$d\sigma_{e,p}/d\Omega=[a_0P_0(\cos\theta_p)+\beta(E_0,E)a_2P_2(\cos\theta_p)]N^{E1}(E_0,E)/E \ , \tag{5}$$

where

$$\beta(E_0,E)=1-3(\alpha/\pi)\frac{(E_f/E_0)^2}{2N^{E1}(E_0,E)} \ ,$$

E_0 and E_f being the energies of the initial and final electron. Here $N^{E1}(E_0,E)$ stands for the plane wave virtual photon spectrum. We replace it by the distorted wave spectrum $N^{E1}(E_0,E,Z)$ to take into account Coulomb distortion effects. (See the Appendix.) Then, in terms of the measured quantity $d\sigma_{e,p}/d\Omega$,

$$\frac{\Gamma_\gamma\Gamma_{p_0}}{\Gamma}=\frac{4a_0E^3}{\pi(\hbar c)^2}\frac{2I_0+1}{2I+1}\frac{d\sigma_{e,p_0}}{d\Omega}\frac{1}{a_0-0.5\beta(E_0,E)a_2N^{E1}(E_0,E,Z)} \ . \tag{6}$$

If we use the value, given in Ref. 12, of $a_2=-0.61$ for the 1^- state at 16.28 MeV, then

$$\frac{\Gamma_\gamma\Gamma_{p_0}}{\Gamma}=4.72\frac{d\sigma_{e,p}/d\Omega}{1+0.305\beta(E_0,E)N^{E1}(E_0,\ 16.28,\ 40)\ \text{eV}} \ . \tag{7}$$

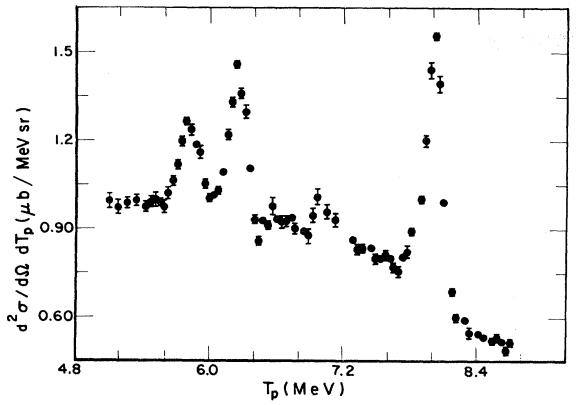

FIG. 4. The proton spectrum measured at $E_0=22$ MeV to determine $\Gamma_{p_2}/\Gamma_{p_0}$. These data have not been corrected for energy loss ($\sim$40 keV) in the target.

For the data taken using the radiator,

$$\frac{\Gamma_\gamma\Gamma_{p_0}}{\Gamma}=3.61\frac{d\sigma_{e+\gamma,p_0}/d\Omega-d\sigma_{e,p_0}/d\Omega}{B(E_0-\Delta E/2,\ 16.28,\ 73)\ \text{eV}}\ , \tag{8}$$

where $B(E_0-\Delta E/2, 16.28, 73)$ represents the number of bremsstrahlung photons produced in the radiator and ΔE is the total electron energy loss in the radiator. Both $N(E_0, 16.28, 40)$ and $B(E_0-\Delta E/2, 16.28, 73)$ in Eqs. (7) and (8) have undergone a small correction, $\leq 1\%$, to take into account the real photons generated in the target.

In order to compare these data with the isochromat of the $E1$ virtual photon spectrum, we have expressed our results in terms of the product $\Gamma_\gamma\Gamma_{p_0}/\Gamma$ for the 16.28 MeV level. In other words, this product has been evaluated from the differential cross section, measured at each electron energy E_0.

The values of $\Gamma_\gamma\Gamma_{p_0}/\Gamma$ obtained from electrodisintegration and photodisintegration are shown in Fig. 5(a) as a function of incident electron energy E_0. They should be independent of E_0 since they are the measure of a nuclear property. The closed circles represent electrodisintegration data (virtual photons), whereas the open circles represent photodisintegration results (real photons). It is apparent that the values of $\Gamma_\gamma\Gamma_{p_0}/\Gamma$ derived in this way from the electrodisintegration experiment fall off with increasing electron energy, whereas the photodisintegration results are close to the average of the electrodisintegration results obtained at the electron energies below 30 MeV.

IV. NUCLEAR SIZE EFFECTS

The discrepancy pointed out above results from the failure of the virtual photon spectra to take into account the nuclear extent. The DWBA virtual photon spectra used to produce Fig. 5(a) take into account the distortion of the incoming and outgoing electron waves in the Coulomb field of a point nucleus. This distortion increases the number of 16.28 MeV virtual photons by 10% for 50 MeV electrons and 7% for 100 MeV electrons. As a result of the finite size of the nucleus the number of virtual photons is decreased with respect to the point-nucleus result. This effect increases with increasing electron energy, atomic number, and multipolarity.

Several procedures[3,14] have recently been suggested for making nuclear size corrections. These all use the plane wave virtual photon spectra to obtain a correction which is then applied to the DWBA spectra.

In the plane wave Born approximation the virtual photon spectra are[15]

$$N_T^{El}(E_0,E)=\frac{\alpha}{4\pi {P_0}^2}\int_{(P_0-P_f)^2}^{(P_0+P_f)^2}\left[\frac{E}{q}\right]^2\left\{\frac{[(P_0+P_f)^2-q^2][q^2-(P_0-P_f)^2]}{(q^2-E^2)^2}+\frac{2q^2}{q^2-E^2}\right\}\left[\frac{q}{E}\right]^{2l}\frac{B(El,q)}{B(El,E)}d(q^2) \tag{9}$$

and

$$N_L^{El}(E_0,E)=\frac{\alpha}{4\pi {P_0}^2}\int_{(P_0-P_f)^2}^{(P_0+P_f)^2}\frac{l}{l+1}\left[\frac{(E_0+E_f)^2}{q^2}-1\right]\left[\frac{q}{E}\right]^{2l}\frac{B(Cl,q)}{B(El,E)}d(q^2)\ , \tag{10}$$

where the subscripts T and L refer to components of the nuclear current perpendicular and parallel to the direction of the momentum transfer $\vec{q}$. Here (p_0,E_0) and (p_f,E_f) are the (momentum, energy), respectively, of the incident and scattered electron. These integrals can be performed analytically if the approximation $qR \ll 1$ is made. Then the transition probabilities in Eqs. (10) and (11) cancel, and we have the plane wave virtual photon spectra.

To obtain a more realistic representation of the virtual photon spectra, the ratios of the transition probabilities can be obtained from some nuclear model. We have used the generalized Helm model[16] for which

$$\frac{B(El,q)}{B(El,E)}=\left[\frac{E}{q}\right]^{2l+2}\frac{{j_l}^2(qR)}{{j_l}^2(ER)}e^{-g^2(q^2-E^2)} \tag{11}$$

and

$$\frac{B(Cl,q)}{B(El,q)}=\left[\frac{E}{q}\right]^{2l}\frac{{j_l}^2(qR)}{{j_l}^2(ER)}e^{-g^2(q^2-E^2)} \tag{12}$$

with the surface thickness parameter g set equal to zero. We have also used a uniform charge distribution assuming Siegert's theorem. Then

$$\frac{B(El,q)}{B(El,E)}=\left[\frac{E}{q}\right]^{2l+2}\frac{\left|\int_0^R j_l(qr)r^2dr\right|^2}{\left|\int_0^R j_l(Er)r^2dr\right|^2} \tag{13}$$

and

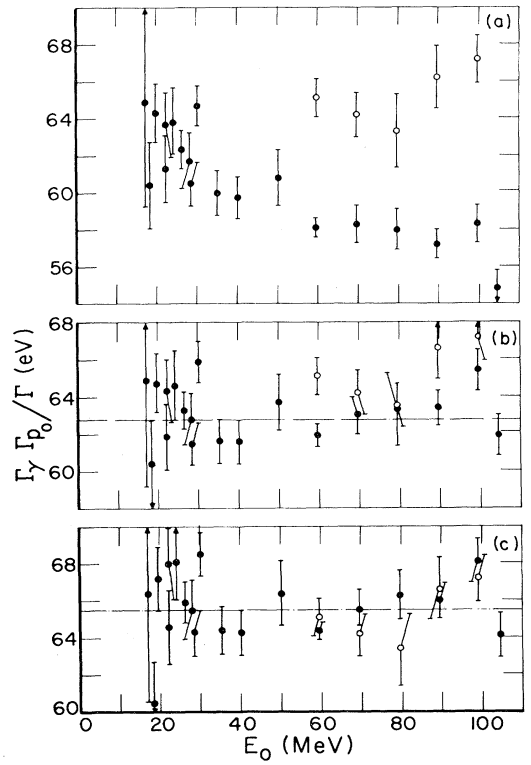

FIG. 5. (a) The quantity $\Gamma_\gamma\Gamma_{p_0}/\Gamma$ vs E_0 obtained using Eqs. (7) and (8). (b) Here the DWBA spectra have undergone a size effect correction using the Helm model. (c) Here the virtual photon spectra evaluated in the second order Born approximation have been used. The horizontal lines in (c) and (d) represent the weighted average values obtained from electrodisintegration.

$$\frac{B(Cl,q)}{B(El,q)} = \left[\frac{E}{q}\right]^{2l} \frac{\left|\int_0^R j_l(qr)r^2dr\right|^2}{\left|\int_0^R j_l(Er)r^2dr\right|^2} . \tag{14}$$

We have used a procedure, developed by Dodge,[17] in which the transition probabilities $B(El,q)$ and $B(Cl,q)$ have been expanded in powers of q^2 and then the integrals in Eqs. (9) and (10) evaluated explicitly term by term. A finite size correction is then obtained by dividing this result by the corresponding point nucleus result. For the electric dipole transition at 16.28 MeV in the ^{90}Zr nucleus this correction for 100 MeV electrons is 0.89 for the Helm model and 0.92 for the uniform charge distribution. Note that had we constrained both models to reproduce the same nuclear charge radius, the corrections would have been somewhat closer. We have applied this correction to the DWBA virtual photon spectrum. This is illustrated in Fig. 6 where we show the 16.28 MeV isochromat of the Zr $E1$ DWBA virtual photon spectrum. The lower curve has applied to it the finite size correction obtained using the Helm model.

In Fig. 5(b) we plot $\Gamma_\gamma\Gamma_{p_0}/\Gamma$ as a function of E_0, having first multiplied the virtual photon spectrum of Eq. (7) by the finite size correction obtained using the Helm model. We see that the size correction has, indeed, removed the downward trend with increasing electron energy seen in Fig. 5(a).

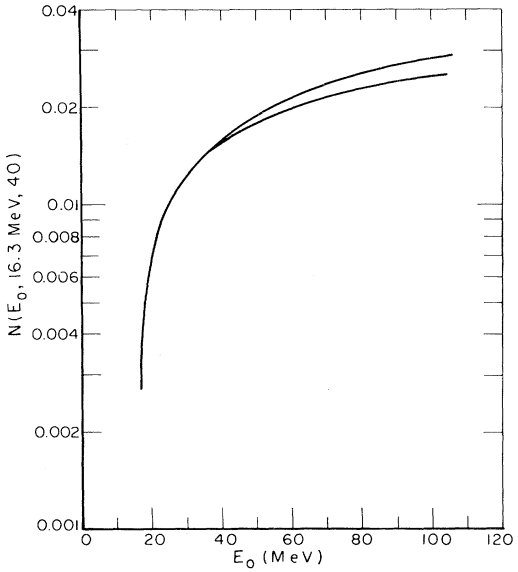

FIG. 6. The 16.28 MeV isochromat of the zirconium $E1$ virtual photon spectrum. The lower curve has applied to it the finite size correction obtained using the Helm model.

Very recently Durgapal and Onley[18] have evaluated the virtual photon spectra in the second order Born approximation (SOBA) using a model for the nuclear charge and current distribution. Their model reproduces values of the charge and transition radii obtained from inelastic electron scattering experiments. Comparison of the DWBA spectra of Soto Vargas *et al.*[2] calculated with a point nucleus with the calculation of Durgapal and Onley shows that the latter are decreased by $\approx 4\%$ for $Z=40$ and $E=16.28$ MeV in the energy range of 20 to 100 MeV due to the effects of an extended charge distribution. The remaining differences between the DWBA virtual photon spectra and Durgapal and Onley's virtual photon spectra arise from the finite nuclear size effects which become important as q becomes manifestly larger than E. Their spectra have been used in Eq. (7) to produce the points plotted in Fig. 5(c).

V. CONCLUSIONS

The $E1$ DWBA virtual photon spectra for zirconium coincide with our experimental results for incident electron energies up to 30 MeV. Certainly, above 50 MeV a correction is needed to take into account the finite extent of the nucleus. A summary of the results is given in Table I, where we show the weighted averaged values of $\Gamma_\gamma\Gamma_{p_0}/\Gamma$ obtained in various ways. The Helm model size correction applied to all of the electrodisintegration data agrees very well with the low energy electrodisintegration results where the size correction is $<2\%$. The uniform charge distribution result does almost as well. The SOBA virtual photon spectra take into account not only what we have called nuclear size effects but also deviations from a point nuclear Coulomb field. Thus, in principle, results

TABLE I. Summary of experimental results. The errors quoted for the present experiment are only statistical. The overall normalization error is ±2 eV.

Reaction	Electron energy range	$\Gamma_\gamma\Gamma_{p_0}$ (eV)
Electrodisintegration	19.77–30.15 MeV (DWBA)	64.7±0.5
	19.77–30.15 MeV (SOBA)	67.1±0.5
Photodisintegration	59.64–99.33 MeV (DBM)	65.4±0.6
Photodisintegration	59.64–99.33 MeV (Schiff)	59.9±0.6
Electrodisintegration with size correction based on the Helm model	19.77–104.40 MeV	63.8±0.3
Electrodisintegration with size correction based on the uniform charge distribution	19.77–104.40 MeV	62.6±0.3
Electrodisintegration using second order Born approximation spectra	19.77–104.40 MeV	66.1±0.3
Result from (e,p) (Ref. 10)		74±10
Result from $^{89}Y(p,\gamma_0)$ (Ref. 12)		78±28

obtained from SOBA virtual photon spectra should be the most reliable. Mean values of $\Gamma_\gamma\Gamma_{p_0}/\Gamma$ obtained from SOBA virtual photon spectra agree best with mean values of $\Gamma_\gamma\Gamma_{p_0}/\Gamma$ obtained from photodisintegration using the Davies-Bethe-Maximon (DBM) bremsstrahlung cross section.[19,20]

The quantity $\Gamma_\gamma\Gamma_{p_0}/\Gamma$ has been determined from the photodisintegration data using both the Davies-Bethe-Maximon formula with Fermi-Thomas model screening functions[19] and the Schiff bremsstrahlung cross section [formula 3BS(e) of Ref. 20]. The result should be the same as that obtained by electrodisintegration, and that obtained using the DBM formula yields a number that is in satisfactory agreement with the electrodisintegration result. The magnitude of the Schiff cross section is excluded by these results.

The errors quoted in Table I are statistical and have meaning relative to each other. There are, however, large errors in the overall normalization which we estimate to be ±3% stemming from the charge measurement, the target nonuniformity, and the determination of $\Delta\Omega(\Delta P/P)$ using National Bureau of Standards standard α-particle sources. Our value for the product, $\Gamma_\gamma\Gamma_{p_0}/\Gamma$, would then be 63.8±1.9 eV using the Helm model or 66.1±2.0 eV using the second order Born approximation spectra. The data from Refs. 10 and 12 are also included in Table I for comparison. These experimental results do not take into account the interference[21] of the analog state with the giant resonance on which it is superimposed. Hasinoff *et al.*[12] have studied this feature of their (p,γ_0) data and have determined that the inclusion of interference decreases the product $\Gamma_\gamma/\Gamma_{p_0}/\Gamma$ by only about 3%. Finally, using our value of 0.58±0.02 for $\Gamma_{p_2}/\Gamma_{p_0}$ and assuming that the 16.3 MeV state decays only through the ground and second excited states of ^{89}Y, the ground-state radiation width is

$$\Gamma_\gamma = 1+(\Gamma_{p_2}/\Gamma_{p_0})(\Gamma_{p_0}\Gamma_\gamma/\Gamma) = 1.58\Gamma_{p_0}\Gamma_\gamma/\Gamma \ .$$

This result translates into 100.8±5.0 eV if we use the Helm model or 104.4±5.2 eV using the second order Born approximation spectra. Hasinoff *et al.*[12] determined both $\Gamma_{\gamma_0}\Gamma_{p_0}$ and Γ from fits to their data. Using $\Gamma_{\gamma_0}\Gamma_{p_0}=6\pm1.5$ keV^2 leads to $\Gamma_{p_0}=60\pm15$ keV while using $\Gamma=77\pm5$ keV leads to $\Gamma_{p_0}=49\pm5$ keV.

ACKNOWLEDGMENTS

The authors wish to acknowledge the joint support of the Conselho Nacional de Desenvolvimento Cientifico e Technologico (Brazil) and the National Science Foundation which has allowed them to collaborate on this project.

APPENDIX

Dodge and Barber[13] were the first to compute $E1$ electrodisintegration angular distributions. Using the formalism of Bosco and Fubini[22] they showed that if the photodisintegration angular distribution were given by

$$\left[\frac{d\sigma}{d\Omega}\right]_\gamma = a_0P_0(\cos\theta_p)+a_2P_2(\cos\theta_p) \ , \tag{A1}$$

then the electrodisintegration angular distribution would be given by

$$\left[\frac{d\sigma}{d\Omega}\right]_e = \{a_0 P_0(\cos\theta_p) + [1 - 3(\alpha/\pi)(E_f/E_0)^2/2N^{E1}]a_2 P_2(\cos\theta_p)\}(N^E E) , \tag{A2}$$

where $N^{E1} = N_T^{E1} + N_C^{E1}$ (Ref. 15). The dependence of the photodisintegration cross section on E is contained implicitly in the angular distribution coefficients a_0 and a_2. However, the nuclear current was not decomposed into transverse and longitudinal components in the formalism of Bosco and Fubini,[22] which makes the incorporation of nuclear size effects difficult, and the multipole expansion was not made in an irreducible representation, which mixes higher multipole components into the dipole. In order to estimate the differences which arise from these deficiencies, we have used as a starting point the coincidence cross section of Drechsel and Überall.[23] For an isolated Breit-Wigner $E1$ resonance in a nucleus of ground state spin $J=0$,

$$\frac{d^3\sigma}{d\Omega_{e'} d\Omega_p dE_f} = \frac{\alpha^2}{\pi^2}\frac{P_f}{P_0}\frac{1}{q_\mu{}^4}\sqrt{3} pER_{\rm BW}(E,\omega) \times \left\{(\mathscr{M}_1)^2 V_L[S^0 P_0(\cos\theta_{p'}) - (2S^2)^{1/2} P_2(\cos\theta_{p'})] + (\mathscr{T}_1^{(e)})^2 V_T\left[S^0 P_0(\cos\theta_{p'}) + \frac{S^2}{\sqrt{2}} P_2(\cos\theta_{p'})\right] - \mathscr{T}_1^{(e)}\mathscr{M}_1 V_I S^2 P_2{}^1(\cos\theta_{p'}) - \frac{1}{2\sqrt{2}}(\mathscr{T}_1^{(e)})^2 (V_S - V_T) S^2 P_2{}^2(\cos\theta_{p'})\right\} ,$$

where

$$V_C = \left[\frac{q_\mu{}^2}{q^2}\right]^2 (E_0 E_f + P_0 P_f \cos\theta_{ee'} + m_e{}^2) ,$$

$$V_T = \frac{\kappa^2}{q^2} + \tfrac{1}{2} q_\mu{}^2 ,$$

$$V_I = \frac{\kappa q_\mu{}^2}{q^3}(E_0 + E_f)\cos\Phi_p , \tag{A3}$$

$$V_S = 2\frac{\kappa^2}{q^2}\cos^2\Phi_p + \tfrac{1}{2} q_\mu{}^2 ,$$

and

$$R_{\rm BW}(E,\omega) = \frac{1}{(E-\omega)^2 + \frac{1}{3}(\Gamma)^2} .$$

In this equation θ'_p is the angle between $\vec{q}$ and $\vec{p}$, and Φ_p is the angle between the $(\vec{q},\vec{P}_0)$ and the $(\vec{q},\vec{P}_f)$ planes, where $\vec{p}$ is the momentum of the emitted nucleon and $\vec{P}_0$ and $\vec{P}_f$ are the momenta of the incident and scattered electrons. The transverse electric inelastic $E1$ form factor is $\mathscr{T}_1^{(e)} = F_T(q,E)$, the longitudinal or Coulomb form factor is $\mathscr{M}_1 = F_C(q,E)$, and $\kappa = \vec{P}_0 \cdot \vec{P}_f$. S^0 and S^2 are the nuclear decay parameters for the decay channels under consideration.[23] The electrodisintegration differential cross section is obtained by integrating Eq. (A3) over the directions of the scattered electron after the transverse and Coulomb form factors are replaced by model dependent expressions or, in the long wavelength approximation (LWA), by their first order expansion terms in q^2R^2, where R is the nuclear charge radius.

The electrodisintegration cross section is given by

$$\frac{d^2\sigma}{d\Omega_p dE_f} = \frac{d^2\sigma_T}{d\Omega_p dE_f} + \frac{d^2\sigma_C}{d\Omega_p dE_f} + \frac{d^2\sigma_{CT}}{d\Omega_p dE_f} + \frac{d^2\sigma_{TT}}{d\Omega_p dE_f} \tag{A4}$$

in the LWA. Note that an electrodisintegration differential cross section contains contributions from all terms in the coincidence cross section and not just from transverse and Coulomb terms as do inelastic electron scattering cross sections. Also note that the electrodisintegration cross section is sensitive to the relative signs of the transverse and Coulomb form factors unlike inelastic electron scattering, and that the relative signs are fixed by current conservation, i.e.,

$$F_C(q,E) \to -\frac{q}{E}\left[\frac{l}{l+1}\right]^{1/2} F_T(q,E)$$

as $q \to E$. Explicitly, the four terms in $d^2\sigma/d\Omega_p dE_f$ are

$$\frac{d^2\sigma_T}{d\Omega_p dE_f} = D\left\{N_T^{E1}(E_0,E)S^0 P_0(\cos\theta_p) + \left[\left[1 + \frac{3m_e{}^2}{2P_0{}^2}\right]N_T^{E1}(E_0,E) - \frac{3}{2}\left[\frac{m_e{}^2}{P_0{}^2}\right]N_L^{E1}(E_0,E) - \frac{3\alpha}{2\pi}\left[\frac{P_f}{P_0}\right]\left[\frac{E_0E_f + m_e{}^2}{P_0{}^2}\right]\right]\frac{S^2}{\sqrt{2}}P_2(\cos\theta_p)\right\} , \tag{A5}$$

$$\frac{d^2\sigma_C}{d\Omega_p dE_f} = D\left[N_C^{E1}(E_0,E)S^0 P_0(\cos\theta_p) + \left\{\left[\frac{1}{4} + \frac{3}{4}\left[\frac{3E_f{}^2 - 2E_0E_f - m_e{}^2}{P_0{}^2}\right]\right]N_C^{E1}(E_0,E) - \frac{3\alpha}{2\pi}\left[\frac{3E_0E_f + m_e{}^2}{P_0{}^2}\right]\right\}\frac{S^2}{\sqrt{2}}P_2(\cos\theta_P)\right] , \tag{A6}$$

$$\frac{d^2\sigma_{CT}}{d\Omega_p dE_f}=3D\left\{\left[\frac{EE_f+m_e{}^2}{P_0{}^2}\right]N_C^{E1}(E_0,E)\right.$$
$$\left.+2\frac{\alpha}{\pi}\left[\frac{P_f}{P_0}\left[\frac{E_0E_f+m_e{}^2}{P_0{}^2}\right]-\frac{m_e{}^2}{P_0{}^2}\left[\frac{E_0(E_0+E_f)}{P_0{}^2}\right]\ln\lambda\right]\right\}\frac{S^2}{\sqrt{2}}P_2(\cos\theta_p)\ , \tag{A7}$$

$$\frac{d^2\sigma_{TT}}{d\Omega_p dE_f}=\tfrac{3}{4}D\left\{\left[1+\frac{E_f{}^2-2E_0E_f-3m_e{}^2}{P_0{}^2}\right]N_C^{E1}(E_0,E)\right.$$
$$\left.-2\frac{\alpha}{\pi}\left[\frac{P_f}{P_0}\left[\frac{E_0E_f+3m_e{}^2}{P_0{}^2}\right]-4\frac{m_e{}^2}{P_0{}^2}\left[\frac{E_0E_f}{P_0{}^2}\ln\lambda\right]\right]\right\}\frac{S^2}{\sqrt{2}}P_2(\cos\theta_p)\ , \tag{A8}$$

where

$$D=\sqrt{3}\alpha pER_{\rm BW}(E,\omega)\,|F_T(E,E)|^2/E^2,\quad \lambda=(E_0E_f+P_0P_f+m_e{}^2)/m_eE\ ,$$

and θ_p is the angle between $\vec{P}_0$ and $\vec{p}$. A factor of $\alpha/[\pi P_0{}^2F_T(E,E)]$ has been absorbed by the virtual photon spectral functions $N_T^{El}(E_0,E)$ and $N_C^{El}(E_0,E)$ in Eqs. (A5)–(A8). Drechsel and Uberall[23] define S^0 to be $\pi\Gamma_p/(\sqrt{3}pE)$; however, to be consistent with the implicit dependence of a_0 and a_2 on E in Eqs. (A1) and (A2), a factor of $R_{\rm BW}(E,\omega)/2\Gamma$ has been included in the definition of S^0. The square of the transverse form factor evaluated at $q=E$ and the photon absorption cross section are related by[24]

$$|F_T(E,E)|^2=E\sigma(E)/(2\pi^2\alpha)=(2E/\pi\alpha)(\Gamma/\Gamma_p)a_0\ . \tag{A9}$$

Combining these factors and using $S^2/S^0=a_2/\sqrt{2}a_0$, we obtain

$$\frac{d^2\sigma}{d\Omega_p dE_f}=\left[a_0P_0(\cos\theta_p)+\left[1+\frac{3}{2}\frac{m_e{}^2}{P_0{}^2}\right]a_2P_2(\cos\theta_p)\right]N^{E1}(E_0,E)$$
$$-\frac{3}{2}\frac{\alpha}{\pi}\left\{\frac{P_f}{P_0}\left[\frac{E_0E_f}{P_0{}^2}\right]+2\frac{m_e{}^2}{P_0{}^2}\left[\frac{E_0(2E_0+E_f)}{P_0{}^2}\ln\lambda-\frac{P_f}{P_0}\right]\right\}a_2P_2(\cos\theta_p)\ . \tag{A10}$$

For $P_0\gg m_e$ this is the result of Dodge and Barber.[13] Terms in the cross section proportional to the Coulomb form factor are strongly dependent on nuclear size effects while terms proportional to the transverse form factor are slightly dependent on these effects.

DWBA and SOBA virtual photon spectra have only been calculated for application to total cross section measurements [see Eq. (1)]; hence the DWBA or SOBA equivalent of Eq. (A10) does not exist. Since the first term of Eq. (A10) only involves $N^{E1}(E_0,E)$ to first order in $(m_e/P_0)^2$, a rigorously correct prescription to correct for Coulomb distortion is to replace $N_{\rm PWBA}^{E1}(E_0,E)$ by $N_{\rm DWBA}^{E1}(E_0,E)$. The second term of Eq. (A10) receives equal and opposite contributions from the Coulomb and transverse terms of the coincidence cross section and a smaller contribution from the Coulomb-transverse interference term. In general, Coulomb distortion effects are largest for the Coulomb terms and smallest for the transverse terms in the coincidence cross section; therefore, Coulomb distortion effects should be larger for the second term than for the first term in Eq. (A10). In order to compensate for the larger Coulomb distortion of the second term we multiplied Eq. (A10) by

$$\frac{N_{\rm DWBA}^{E1}(E_0,E)}{N_{\rm PWBA}^{E1}(E_0,E)}\ .$$

The ultimate justification for this procedure is that the second term in our kinematic situation is always less than 2% of the first term.

*On leave from the University of Sao Paulo, Sao Paulo, Brazil.

[1]W. W. Gargano and D. S. Onley, Phys. Rev. C 4, 1032 (1971).
[2]C. W. Soto Vargas, D. S. Onley, and L. E. Wright, Nucl. Phys. A288, 45 (1977).
[3]E. Wolynec, W. R. Dodge, R. G. Leicht, and E. Hayward, Phys. Rev. C 22, 1012 (1980).
[4]W. R. Dodge, R. G. Leicht, E. Hayward, and E. Wolynec, Phys. Rev. C 24, 1952 (1981).
[5]D. M. Skopik, J. Asai, and J. J. Murphy II, Phys. Rev. C 21, 1746 (1980).
[6]T. Tamae, T. Urano, M. Hirooka, and M. Sugawara, Phys. Rev. C 21, 1758 (1980).
[7]A. G. Flowers, D. Branford, J. C. McGeorge, A. C. Shotter, P. Thorley, and C. H. Zimmerman, Phys. Rev. Lett. 43, 323

(1979).
[8]E. Hayward, in *Giant Multipole Resonances,* edited by Fred E. Bertrand (Harwood Academic, New York, 1980).
[9]H. Ströher, R. D. Fischer, J. Drexler, K. Huber, U. Kneissl, R. Ratzek, H. Ries, W. Wilke, and H. J. Maier, Phys. Rev. Lett. 47, 318 (1981); Nucl. Phys. A378, 237 (1982).
[10]K. Shoda, M. Sugawara, T. Saito, and H. Miyase, Nucl. Phys. A221, 125 (1974).
[11]W. M. Mason, G. Kernel, J. L. Black, and N. W. Tanner, Nucl. Phys. A135, 193 (1969).
[12]M. Hasinoff, G. A. Fisher, and S. S. Hanna, Nucl. Phys. A216, 221 (1973).
[13]W. R. Dodge and W. C. Barber, Phys. Rev. 127, 1742 (1962).
[14]A. C. Shotter, J. Phys. G 5, 371 (1979).
[15]R. H. Dalitz and D. R. Yennie, Phys. Rev. 105, 1598 (1957).
[16]M. Rosen, R. Raphael, and H. Überall, Phys. Rev. 163, 927 (1967).
[17]W. R. Dodge (unpublished).
[18]P. Durgapal and D. Onley, Bull. Am. Phys. Soc. 27, 487 (1982); P. Durgapal, Ph.D. dissertation, Ohio University, Athens, Ohio, 1982; private communication.
[19]J. L. Mathews and R. O. Owens, Nucl. Instrum. Methods 111, 157 (1973).
[20]H. W. Koch and J. W. Motz, Rev. Mod. Phys. 31, 920 (1959).
[21]H. Ejiri, P. Richard, S. Ferguson, R. Heffner, and D. Perry, Nucl. Phys. A128, 388 (1969).
[22]B. Bosco and S. Fubini, Nuovo Cimento 9, 350 (1958).
[23]Dieter Dreschel and H. Überall, Phys. Rev. 181, 1383 (1969).
[24]James S. O'Connell, in Electromagnetic Nuclear Interactions: I. Introduction, Operators, and Sum Rules, National Bureau of Standards Internal Report 82-2547, 1982, p. 66.